Impacts of pressure to the structural, electronic and magnetic properties of Dirac semimetal $EuMnBi_2$

Resta A. Susilo,[1,*,†] Wen Deng,[1,†] Jiajia Feng,[1] Aifeng Wang,[2,‡] Naomi Kawamura,[3] Naoki Ishimatsu,[4] Saori Kawaguchi,[3] Mingzhi Yuan,[1] He Li,[1] Weijun Ren,[5] Takeshi Nakagawa,[6] Cedomir Petrovic,[2] and Bin Chen[1,§]

[1]*Center for High Pressure Science and Technology Advanced Research, Shanghai 201203, China*
[2]*Condensed Matter Physics and Materials Science Department, Brookhaven National Laboratory, Upton, New York 11973, USA*
[3]*Japan Synchrotron Radiation Research Institute, Sayo, Hyogo 679-5198, Japan*
[4]*Graduate School of Advanced Science and Engineering, Hiroshima University, Higashihiroshima, Hiroshima 739-8526, Japan*
[5]*Shenyang National Laboratory for Materials Science, Institute of Metal Research, Chinese Academy of Sciences, Shenyang 110016, China*
[6]*Center for High Pressure Science and Technology Advanced Research, Beijing 100094, China*

(Received 23 June 2021; revised 28 August 2021; accepted 23 September 2021; published 11 October 2021)

We report our investigations on the effects of pressure on the electronic and magnetic properties of magnetic Dirac semimetal $EuMnBi_2$ by using electrical transport, synchrotron x-ray diffraction, and x-ray absorption spectroscopy. The antiferromagnetic interaction due to the Eu magnetic moment in $EuMnBi_2$ is enhanced under pressure up to ~3.9 GPa. The Néel temperature (T_N) is found to disappear above 4 GPa and a new transition T_t at around 29 K emerges above 6 GPa. T_t remains relatively constant up to 15 GPa, above which it increases with further compression, reaching ~60 K at 22 GPa. Eu L-edge x-ray absorption spectroscopy revealed a valence change of Eu toward a trivalent state that begins above 6 GPa, which indicates that T_t is likely related to the valence transition temperature of Eu. Sign reversal of the Hall resistivity above 7 GPa suggests that the valence change of Eu also induces a Fermi surface modification.

DOI: 10.1103/PhysRevResearch.3.043028

I. INTRODUCTION

Dirac materials, in which the low-energy electrons obey the relativistic Dirac equation, are currently attracting large attention [1,2]. The linear dispersion, massless and chiral excitation of the Dirac cone, as well as the high mobility of the Dirac fermions in Dirac materials give rise to a number of quantum transport phenomena under applied magnetic field which is of interest for spintronic applications.

Among Dirac materials, the $AMnBi_2$ (A = Ba, Ca, Sr, Eu, and Yb) compounds have stood out as unique system due to the coexistence of the linear Dirac band and the magnetic order of the Mn^{2+} ion (e.g., [3–17]). The coupling between the Dirac fermions and magnetic order provides a natural platform to study the effects of magnetism on tuning the topological bands. $EuMnBi_2$, a member of the $AMnBi_2$ compounds, was reported to possess unique electronic properties owing to the coupled interaction between the Dirac fermions hosted by the Bi square nets and the magnetism of the Mn and Eu magnetic moments [7,12]. $EuMnBi_2$ crystallizes in the tetragonal $I4/mmm$ space group similar to $SrMnBi_2$ [3,4]. The structure consists of a MnBi layer with edge-sharing $MnBi_4$ tetrahedrons and a Bi square net sandwiched with Eu atoms [Fig. 1(a)]. The antiferromagnetic ordering of the Eu sublattice occurs at low temperature of $T_N = 22$ K [7,12]. As a special case in the $AMnBi_2$ compounds, the transport behavior and Fermi surface topology of $EuMnBi_2$ are strongly influenced by the magnetism of the Eu atom. Quantum Hall effect is observed by tuning the antiferromagnetic order of the Eu moment under high magnetic field, a characteristic of interest to spintronics [12].

High-pressure studies on Dirac semimetals are currently attracting significant interest, as pressure may drive the Dirac semimetal state into a new quantum state with novel properties. The current interest lies in the possibility to induce the topological superconductivity which is believed to host a Majorana fermion [18–21]. The coexistence of the topological band structure and magnetism in the $AMnBi_2$ compounds can be expected to generate novel physical states under compression, making this system fundamentally attractive to explore at high pressures. However, high-pressure studies on the $AMnBi_2$ system remains scarce. Due to the structural similarity with the Fe pnictide (Pn) superconductors, $SrMnBi_2$ has been proposed to be a possible superconductor under pressure or chemical doping [4]; however no pressure studies have been reported so far. To date, only $BaMnBi_2$ has been studied under pressure, revealing the pressure-induced

*resta.susilo@hotmail.com; Present address: Department of Physics, Pohang University of Science and Technology, Pohang 37673, Korea.
†These authors contributed equally to this work.
‡Present address: College of Physics, Chongqing University, Chongqing 401331, China.
§chenbin@hpstar.ac.cn

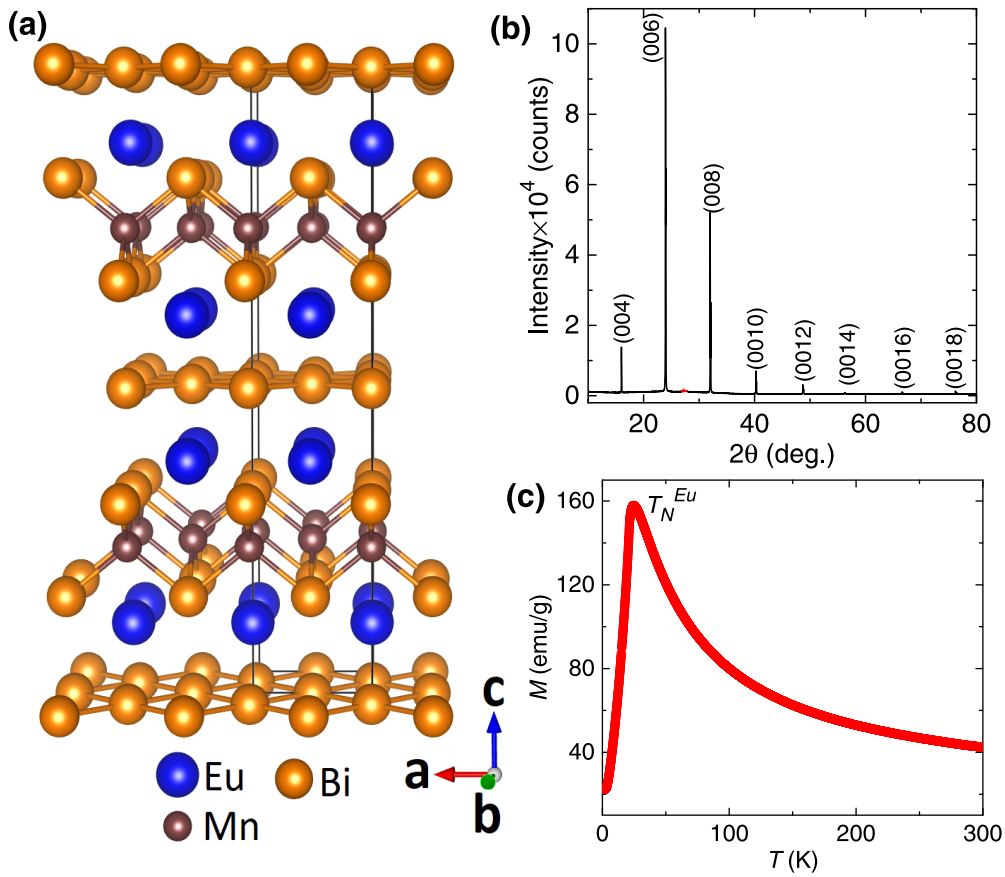

FIG. 1. (a) Crystal structure of $EuMnBi_2$. (b) Single-crystal x-ray diffraction pattern and (c) magnetization of $EuMnBi_2$. Magnetization data were collected in the field-cooled mode with the applied magnetic field H of 1000 Oe parallel to the c axis.

superconductivity with $T_c \sim 4$ K at 2.6 GPa [22]. However, the superconductivity might be induced due to the excess of Bi flux at the surface/sample interface, as reported in the polycrystalline $SrMnBi_2$ at ambient pressure [23].

In this paper, we report our investigations on the effects of pressure on the electronic, structural, and magnetic properties of $EuMnBi_2$ with the particular emphasis on the low-temperature properties related to the magnetism of Eu. We found that the T_N of Eu is enhanced with pressure up to ~3.9 GPa. Further compression leads to the disappearance of T_N. Another low-temperature transition at $T_t \sim 28$ K appears above 6 GPa which we attribute to the Eu valence transition temperature. Synchrotron x-ray diffraction and spectroscopy revealed a pressure-induced transition of Eu above 7 GPa without structural transformation. This valence transition also induces a modification of the Fermi surface as indicated by the sign change of Hall resistivity.

II. METHODS

Single crystals of $EuMnBi_2$ were grown using a high-temperature self-flux method, following the procedure described previously [7]. The resistivity data at high pressure were measured up to ~22 GPa in a homemade multifunctional measurement system (Cryomagnetics, Inc.) using a diamond anvil cell (DAC) made of a Be-Cu alloy. The size of the diamond culet used was 300 μm in diameter. The $EuMnBi_2$ single crystal was cut into a square of ~60 μm in width with 15 μm in thickness. NaCl was used as a pressure medium for run 1 whereas for run 2, soft hBN powder was used. We used the van der Pauw four-probe method to measure electrical resistance by using platinum (Pt) foil as electrodes.

Synchrotron x-ray diffraction measurements were carried out at beamline BL10XU in SPring-8 ($\lambda = 0.4138$ Å). Pressure was generated using a symmetric DAC using a stainless steel gasket and silicon oil as a pressure-transmitting medium. High-pressure Eu L_3-edge x-ray absorption spectroscopy in the high-energy resolution fluorescence detected mode (HERFD-XAS) using three Ge(333) spherically bent analyzer crystals was measured at the BL39XU beamline in SPring-8. The sample was loaded in a DAC with glycerin as a pressure-transmitting medium. In all cases, pressure calibrations were performed using the fluorescence from ruby chips [24] loaded with the sample inside the DAC. The Le Bail fitting to the x-ray diffraction patterns was accomplished using the FullProf/WinPLOTR software [25,26].

III. RESULTS AND DISCUSSION

The as-grown crystals are platelike and the basal plane of the cleaved crystal is the crystallographic ab plane as revealed from the single-crystal XRD pattern [Fig. 1(b)]. Magnetization data show a cusplike behavior at $T_N = 22$ K which corresponds to the antiferromagnetic ordering of the Eu

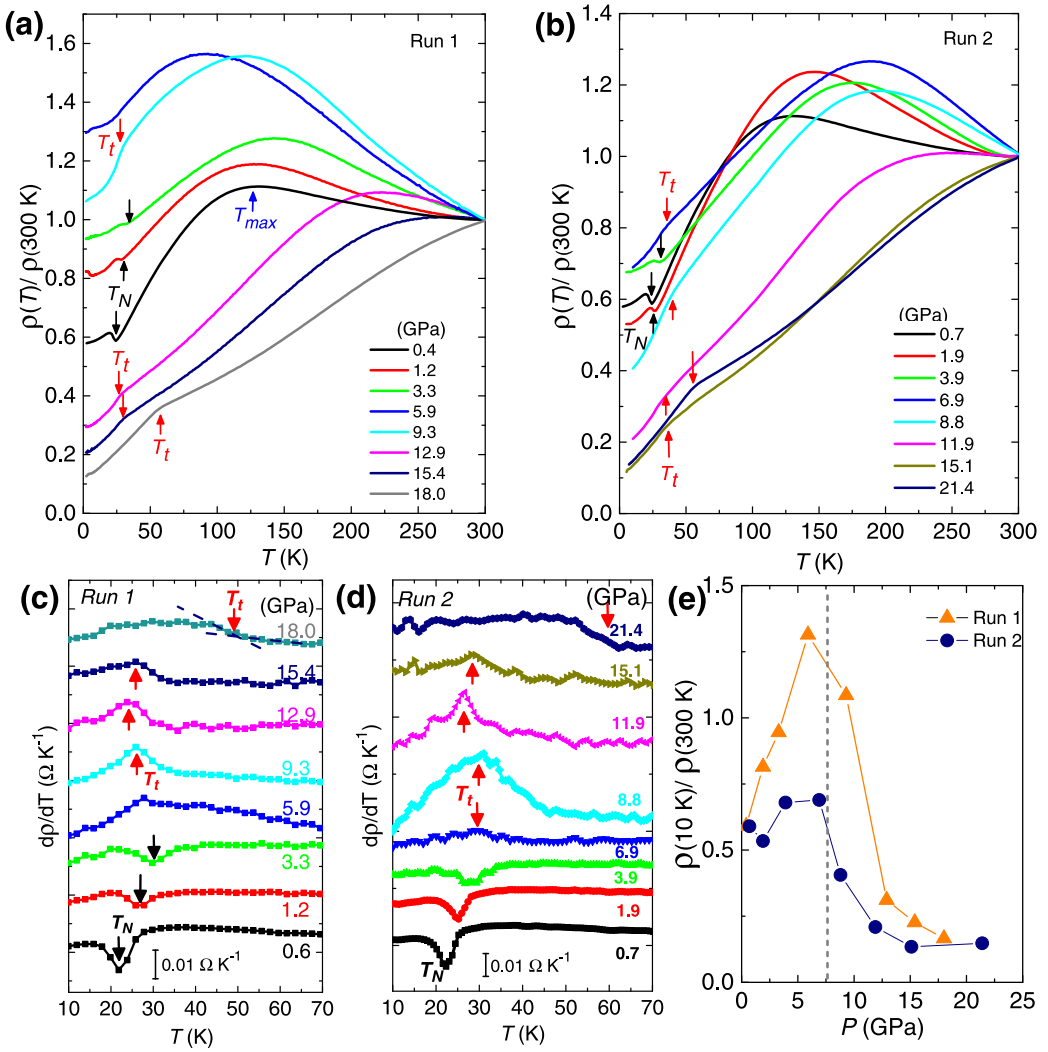

FIG. 2. Temperature dependencies of the normalized resistivity $[\rho(T)/\rho(300\,\mathrm{K})]$ of $EuMnBi_2$ measured at various pressures obtained from run 1 (a) and run 2 (b), respectively. Temperature derivative of the resistivity data of $EuMnBi_2$ at various pressures for run 1 (c) and run 2 (d). Black and red arrows indicate T_N and T_t, respectively, as discussed in the main text. (e) Normalized resistivity $[\rho(5\,\mathrm{K})/\rho(300\,\mathrm{K})]$ plotted against pressure. (e) Pressure dependence of T_{max} in $EuMnBi_2$.

magnetic moment [Fig. 1(c)], in agreement with previous results [7,12].

In Figs. 2(a) and 2(b), we show the temperature dependence of the normalized in-plane resistivity $[\rho(T)]$ of $EuMnBi_2$ measured at various pressures up to ∼21 GPa for two different runs. At 0.4 GPa and 0.7 GPa, a clear anomaly in the resistivity data is observed at $T_N = 22$ K which corresponds to the antiferromagnetic ordering temperature of the Eu magnetic moment, consistent with the magnetization data. In addition, we also observed a broad maximum centered at $T_{\mathrm{max}} \sim 125$ K that is unclear in origin. One possibility is that T_{max} appears due to the contamination of the out-of-plane (interlayer) component of the resistivity. Such a broad maximum was observed in the out-of-plane resistivity of an isostructural $SrMnBi_2$ and related to a crossover from high-T incoherent to low-T coherent conduction [3]. It is also possible that this broad maximum is related to the Eu valence instability, as commonly observed in the mixed valent Eu compounds [27,28]. In the mixed valent Eu compounds, the system can be considered as an alloy that contains both Eu^{2+} and Eu^{3+} ions, each with p_2 and p_3 occupation probabilities. At a given temperature, the minority Eu ion acts as an impurity to the scattering potential for the conduction electrons that fluctuates, since the Eu ions are fluctuating between the two valence states. A resistivity maximum then appears at a temperature where the scattering of the conduction electrons is the largest, i.e., where the largest fluctuation between the two valence states occurs [27,29].

With increasing pressure, T_N shifts to higher temperatures as indicated by the minimum in the temperature-derivative data [Figs. 2(c) and 2(d)]. This indicates that the antiferromagnetic interaction between the Eu magnetic moment is enhanced with pressure to ∼3 GPa. Above 4 GPa, the peak in the resistivity data related to T_N disappears and no low-temperature feature was observed at 5.9 GPa. At 6.9 GPa a new inflection point at $T_t = 28$ K emerges, suggesting a pressure-induced transition at low temperature. Such transition is also reflected in the temperature-derivative data,

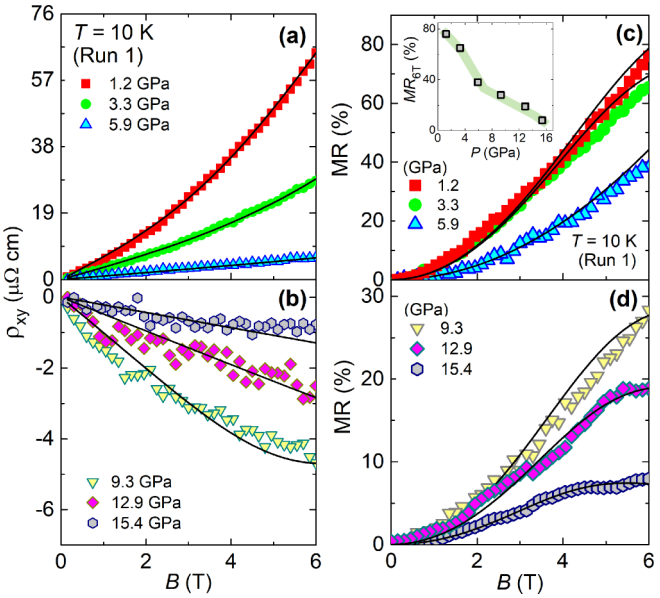

FIG. 3. Magnetic field dependencies of (a), (b) the Hall resistivity (ρ_{xy}) and (c), (d) magnetoresistance (MR) of $EuMnBi_2$ at 10 K measured at various pressures for run 1. Inset in (c) shows the pressure dependence of MR at 6 T. Solid lines are fits to the data using a two-band model, as described in the text.

where the minimum derivative corresponding to T_N changes to a maximum peak in the temperature-derivative data [see Figs. 2(c) and 2(d)]. On increasing pressure, T_t does not change significantly and is relatively constant at around 26 K up to ~15 GPa, above which it is enhanced, reaching $T_t \sim 50$ K at 21.4 GPa. The change in the low-temperature resistivity of $EuMnBi_2$ above 6 GPa is also accompanied by other observations. For instance, the normalized low-temperature resistivity ($\rho_{10\,K}/\rho_{300\,K}$) shows a considerable decrease above 6 GPa [Fig. 2(c)] and becomes almost constant above 12 GPa. The broad maximum in the resistivity (T_{max}) also tends to shift toward higher temperatures with increasing pressure, in particular on compression above 6 GPa. We note that the crystal used in the resistivity measurements was carefully cleaved prior to experiments, thus minimizing the contribution from Bi impurity commonly formed on the surface of the crystal. No superconducting transition that could be related to the pressure-induced superconductivity of Bi [30] was observed in either run. The absence of superconductivity in $EuMnBi_2$ is also in contrast to that reported to occur in the isostructural $BaMnBi_2$ above 2 GPa [22].

Hall resistivity (ρ_{xy}) data were then measured to give deeper insights into the change of the transport behavior under pressure. As presented in Figs. 3(a) and 3(b), the field dependence of ρ_{xy} of $EuMnBi_2$ measured at $T = 10$ K exhibits a linear characteristic at low fields. However, the nonlinear behavior at higher fields indicates a multiband transport, in agreement with previous reports [7] and also similar to those observed in $SrMnBi_2$ [31], $YbMnSb_2$ [32], and $EuZnSb_2$ [33]. $\rho_{xy}(H)$ exhibits a positive slope below 9 GPa suggesting dominant hole carriers. $\rho_{xy}(H)$ becomes negative above 9 GPa, a pressure similar to that at which T_t appears that indicates a crossover from the hole-dominated carrier to the electron-dominated one. The magnetoresistance ratio (MR = $\Delta\rho_{xx}/\rho_{xx}$) of $EuMnBi_2$ at 10 K under various pressures is presented in Figs. 3(c) and 3(d). The MR ratio is ~77% at 1.2 GPa and 6 T which gradually decreases on increasing pressure, reaching ~8% at 15.4 GPa. The magnitude of MR at 6 T varies nonlinearly with pressure as evident from the slope change occurring above 6 GPa [inset of Fig. 3(c)]. Interestingly this change in slope takes place at the same pressure where the Hall resistivity changes its sign suggesting that the change in the dominant carrier from hole to electron above 6 GPa also affects the MR of $EuMnBi_2$.

In order to understand the sign change of Hall resistivity and change in the MR data under pressure, we employed a semiclassical two-band model to fit both data [34,35]:

$$\rho_{xy} = \frac{B}{e}\frac{\left(n_h\mu_h^2 - n_e\mu_e^2\right) + (n_h - n_e)(\mu_h\mu_e)^2B^2}{(n_h\mu_e + n_e\mu_h)^2 + [(n_h - n_e)(\mu_h\mu_e)B]^2}, \quad (1)$$

$$\mathrm{MR} = \frac{n_e\mu_e n_h\mu_h(\mu_h + \mu_e)^2B^2}{(n_h\mu_e + n_e\mu_h)^2 + [(n_h - n_e)(\mu_h\mu_e)B]^2}, \quad (2)$$

where n_h (n_e) and μ_h (μ_e) represent the carrier concentrations and mobilities of holes (electrons), respectively. The solid lines in Fig. 3 are the fitted curves to both $\rho_{xy}(H)$ and MR. The fits to the MR data below 5 GPa can be considered the worst among the whole data set, most probably due to the omission of the contribution from the Eu magnetic ordering. Despite the number of simplifying assumptions, e.g., field-independent parameters, and no effects from the spin-flop transition of Eu magnetic moment to the Hall coefficients and MR, the quality of the fits is satisfactory.

The derived carrier concentrations and mobilities of $EuMnBi_2$ as a function of pressure are presented in Fig. 4. We found that the best fits to the data below 6 GPa are obtained considering the n_h/n_e ratio of slightly above 1. For example at 1.2 GPa, n_h and n_e are 3.2×10^{19} cm^{-3} and 3.0×10^{19} cm^{-3}, respectively, whereas the mobilities are around 2.3 $cm^2\,V^{-1}\,s^{-1}$ and 1.2 $cm^2\,V^{-1}\,s^{-1}$ for holes and electrons, respectively. The hole concentrations remain the dominant carrier transport in $EuMnBi_2$ up to 6 GPa. Above 6 GPa, both hole and electron concentrations show dramatic increases; however the concentration of electrons is now higher than that of holes, i.e., $n_h = 4.4 \times 10^{20}$ cm^{-3}, $n_e = 6.3 \times 10^{20}$ cm^{-3} at 9.3 GPa. Further increasing pressure leads to a decrease of hole concentration and a steady increase of electrons concentration which indicates that the electron becomes the dominant transport carrier in $EuMnBi_2$ above 6 GPa. In line with the dominant carrier switching, drastic change of the mobilities is also observed above 6 GPa [Fig. 4(b)]. In particular, the electron mobility increases by almost 2 orders of magnitude reaching the maximum value of ~34 $cm^2\,V^{-1}\,s^{-1}$, whereas the hole mobility significantly decreases to around 3×10^{-3} $cm^2\,V^{-1}\,s^{-1}$ at 12.9 GPa. This result indicates that the increase of electron concentration and mobility gives rise to the sign reversal of ρ_{xy} above 6 GPa.

To determine the possible origin of carrier switching in $EuMnBi_2$ above 6 GPa, we then measured the Eu L_3-edge x-ray absorption spectra by using high-energy resolution fluorescence detected mode (HERFD-XAS) at various pressures as shown in Fig. 5(a). Two distinct peaks are observed around 6.975 keV and 6.983 keV in all HERFD-XAS spectra,

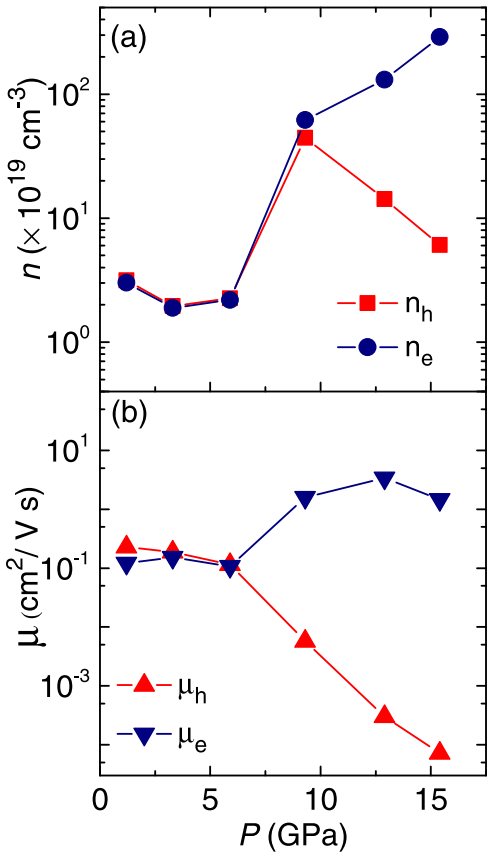

FIG. 4. Carrier concentrations (a) and mobilities (b) of $EuMnBi_2$ as a function of pressure.

representing the $4f$ electron configuration for Eu^{2+} ($4f^7$) and Eu^{3+} ($4f^6$), respectively. The relative intensities of Eu^{2+} and Eu^{3+} contributions are determined by fitting the HERFD-XAS spectra with a two-component model consisting of an arctangent step function and a Lorentzian peak for each valence state. The mean Eu valence (v) was estimated by $v = 2 + (\frac{I(3+)}{I(2+)+(I(3+)})$, where $I(2+)$ and $I(3+)$ represent the intensities of the Eu^{2+} and Eu^{3+} contributions, respectively.

The derived mean Eu valence in $EuMnBi_2$ at ambient condition is ~2.2+, which is higher than the expected divalent Eu state. While such valence state seems to be in contradiction with the localized $4f$ electrons of Eu^{2+} behavior observed in the magnetization and specific heat data [7,12], we note that the saturated Eu magnetic moment measured in high applied field above 30 T is less than 7 μ_B (i.e., ~6.4 μ_B [12]). The decrease in Eu moment possibly reflects the decrease in the number of Eu^{2+} ions leading to a deviation from the divalence state. In the simple ionic model [36], the saturated Eu moment corresponds to a Eu valence of about 2.1, which is close to our derived Eu valence. This suggests that Eu in $EuMnBi_2$ is not in a pure divalent state, but rather is in an intermediate valence state close to 2+ at ambient pressure.

The mean Eu valence remains within around 2.2 below 5 GPa. On increasing pressure above 6 GPa, the relative intensity of the Eu^{3+} contribution increases compared to the Eu^{2+} contribution that leads to the increase of the mean Eu valence in $EuMnBi_2$. The mean Eu valence increases steadily with increasing pressure, reaching the value of ~2.6 at 20 GPa, above which it becomes relatively constant. This indicates that Eu in $EuMnBi_2$ undergoes pressure-induced valence transition above 6 GPa. However, a trivalent Eu state is not realized up to the highest measurement of around 20 GPa.

The valence transition in the Eu-based compounds under pressure can be expected, since the Eu^{3+} ion has a smaller ionic radius than Eu^{2+}, and such valence transition is driven by the continuous contraction of the unit cell volume of the crystal under pressure. We then carried out synchrotron x-ray diffraction measurements on pulverized $EuMnBi_2$ up to 18 GPa as presented in Fig. 6(a) to investigate the structural stability under pressure. The diffraction pattern at 1.2 GPa revealed that the pulverized sample contains additional impurities, mostly unreacted Bi, and another unidentified phase that can be indexed with a cubic $Fm\bar{3}m$ space group and the lattice parameter of $a = 4.954(3)$ Å (at 1.2 GPa). Our attempt to search for a possible phase with similar lattice parameters did not give any satisfactory conclusion. Possible cubic oxides such as EuO and β-BiO are found to have larger lattice parameters; therefore in the end we attributed this to an unknown phase. We estimate that this unknown impurity phase accounts for 5 wt. % or less. Although the contribution of this unknown phase to the XAS spectra, if it contains Eu ions, cannot be fully excluded, such a rather small impurity phase cannot account for a large increase in the Eu valence from ~2.2 below 10 GPa to ~2.6 at 20 GPa, which lead us to attribute such valence transition to be intrinsic from $EuMnBi_2$ sample.

The diffraction patterns undergo several changes on increasing pressure. However the changes can be properly tracked and attributed to the structural transformation of Bi [37–39] [see Fig. 6(b)]. The pressure dependence of the derived unit cell volume of the Bi impurity phase is found to match well with previous reports (Fig. 8), indicating that the changes in the diffraction patterns are not related to the structural transformation of $EuMnBi_2$. The three strongest peaks (112), (008), and (200) belonging to the $I4/mmm$ space group of $EuMnBi_2$ at $2\theta \sim 7.7°$, 8.7°, and 10.6°, respectively, shift to higher angles due to the contraction of the unit cell under pressure. All diffraction patterns can be fitted with the $I4/mmm$ space group until 18 GPa [Fig. 6(b)], which suggests the absence of structural phase transition in the compressed $EuMnBi_2$. The unit cell volume and lattice parameters of $EuMnBi_2$ derived from the Le Bail fitting are shown in Figs. 6(c) and 6(d), respectively. The derived unit cell volume can be fitted well by the third-order Birch-Murnaghan equation of state [40,41] yielding a zero-pressure volume $V_0 = 231.1(5)$ Å, bulk modulus $B_0 = 41.8(4)$ GPa, and its first derivative $B_0' = 4.1$.

In Fig. 7, we show the pressure-temperature (P-T) phase diagram of $EuMnBi_2$, with particular emphasis on the low-temperature region ($T < 60$ K). The antiferromagnetic transition of Eu increases from 22 K at 0.4 GPa to ~31 K at 3.9 GPa. In most magnetic systems, the application of pressure usually weakens the magnetism that leads to the suppression of magnetic-ordering transition due to electron delocalization (e.g., [42–44]). The increase of T_N in $EuMnBi_2$ with pressure suggests that the Eu-Eu magnetic coupling, governed by the RKKY exchange interaction, is enhanced

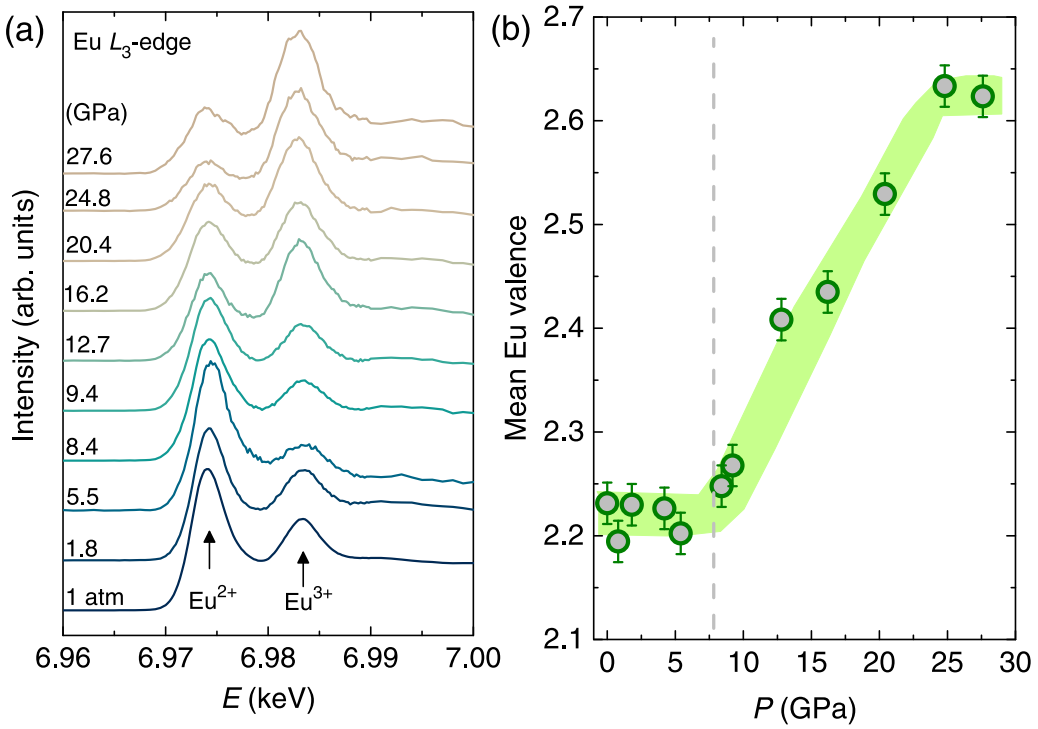

FIG. 5. (a) Room temperature Eu L_3-edge HERFD-XAS spectra of $EuMnBi_2$ at various pressures. (b) The derived mean valence of Eu as a function of pressure. Dashed line is a guide to the eyes.

with pressure. In particular, the enhanced T_N is possibly driven by the enhancement of the intralayer (direct) exchange coupling due to the reduction of the in-plane interatomic distances with pressure. A similar case was also recently observed in $EuIn_2As_2$ where the enhancement of the intralayer exchange interaction dominates the interlayer coupling leading to a giant enhancement of T_N under pressure [45].

On further compression, the anomaly in $\rho(T)$ related to T_N vanishes that indicates a sudden suppression of Eu antiferromagnetism. T_N is replaced by a new transition at T_t that emerges above 6 GPa. The appearance of a new low-temperature transition in $EuMnBi_2$ is similar to the case of $EuFe_2As_2$ where the antiferromagnetic state of Eu transforms to a ferromagnetic (FM) state above ∼6 GPa [46]. If T_t in $EuMnBi_2$ was related to a new magnetic transition, probably ferromagnetic transition of Eu, the increase of T_t at higher pressure suggest that the Eu-Eu exchange coupling is further enhanced by pressure. This is in contrast to the Eu L_3-edge HERFD-XAS spectra that shows a pressure-induced Eu valence transition above 6 GPa. Such valence change to a nonmagnetic trivalent state tends to weaken magnetism and favor a nonmagnetic ground state. Indeed, the pressure-induced AFM to FM state in $EuFe_2As_2$ occurs in the pressure range where the Eu^{2+} state is still stable and further compression led to the suppression of the FM state due to the valence transition above 10 GPa [46]. One possibility is that T_t in $EuMnBi_2$ above 6 GPa is related to the valence transition temperature.

The transformation from AFM transition to valence transition temperatures in the Eu-based compounds under pressure is not uncommon behavior. Several compounds such as $EuRh_2Si_2$ and $EuNi_2(Ge_{1-x}Si_x)_2$ were reported to undergo first-order valence transition under pressure where the AFM transition temperature disappears and is replaced by the valence transition temperature (T_v) on further compression [28,29,47,48]. In those compounds, the Eu valence increases from a nearly divalent state ($Eu^{2+\delta}$) at high temperature above T_v to a nearly trivalent state ($Eu^{3-\delta}$) below T_v ($\delta, \delta' < 1$). Such observation is similar to our findings in which T_N is replaced by T_t above 6 GPa where the pressure-induced valence transition begins based on our HERFD-XAS measurements. This evidence suggests that T_t in $EuMnBi_2$ above 6 GPa is likely related to the valence transition temperature. Synchrotron x-ray diffraction measurements at room temperature rule out a possible phase transition above 6 GPa indicating that the valence transition is not accompanied by the change in the crystal structure. The temperature dependence of the Eu L_3-edge HERFD-XAS measurements on $EuMnBi_2$ above 6 GPa would undoubtedly be useful to confirm this proposed scenario.

It is known that the transport behavior of the $AMnBi_2$ family is dictated by the p electrons of Bi square nets that host quasi-two-dimensional Dirac fermions. In the case of $EuMnBi_2$, the Eu ionic layers adjacent to the Bi square net play an important role and give rise to a coupled interaction between magnetism and transport behavior [7,12]. Therefore, the anomalous change in the field-dependent Hall resistivity data can also be related to the valence change of Eu observed from the HERFD-XAS measurements. As shown in Figs. 3(a) and 3(b), the sign of Hall resistivity changes above ∼6 GPa suggesting a possible change in the electronic structure accompanying the valence transition. A common explanation for the change in the sign of Hall resistivity, from positive to negative, is the switching of the dominant charge carriers

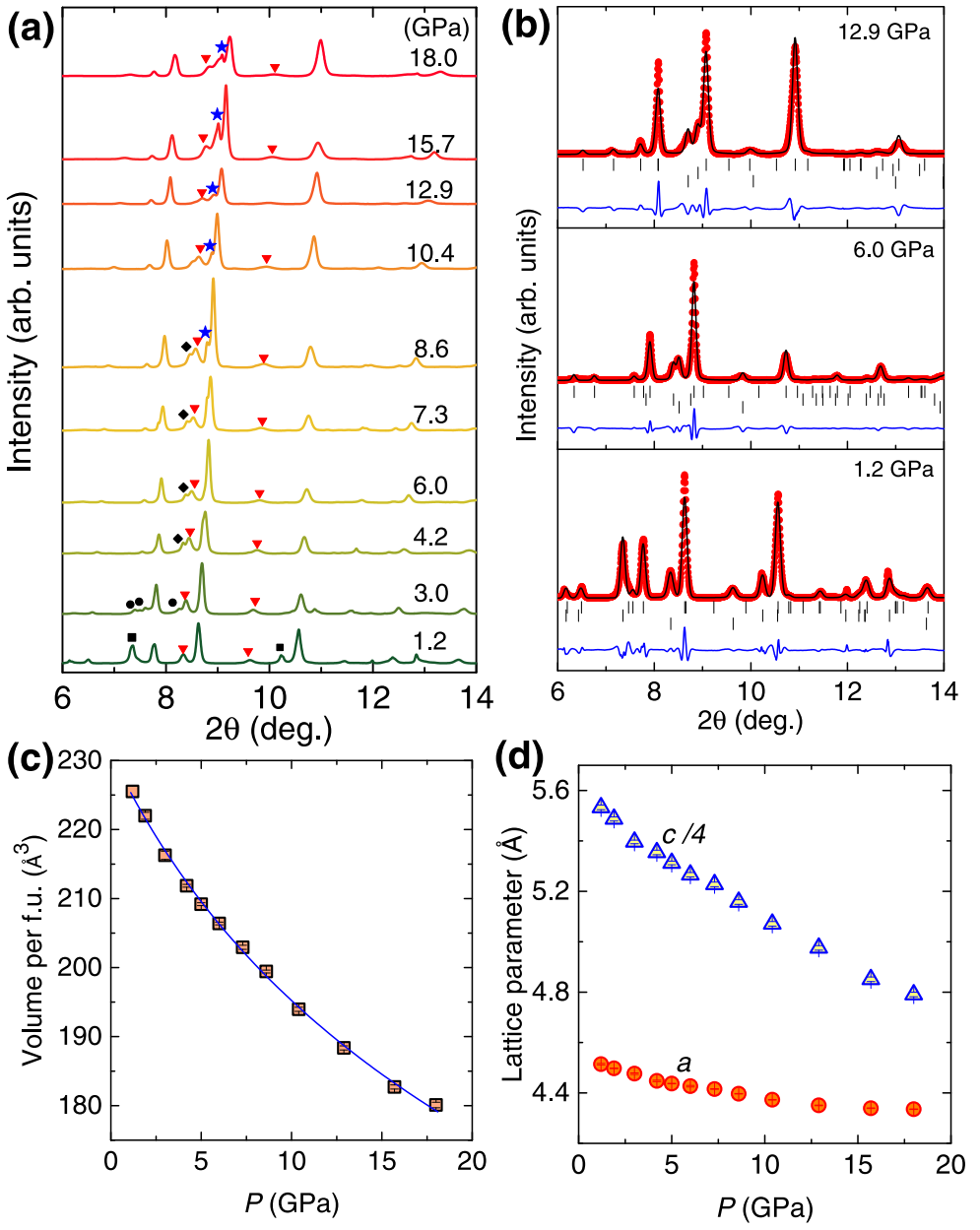

FIG. 6. (a) Room temperature x-ray diffraction patterns of $EuMnBi_2$ taken at various pressures. □, ◯, ◊, ⋆, and ▽ symbols represent Bi-I, Bi-II, Bi-III, Bi-V, and unknown phases, respectively. (b) Representative refinement of the x-ray diffraction patterns. The rows of Bragg markers, from top to bottom, represent $EuMnBi_2$, Bi impurity, and unknown phase, respectively. Note that the second Bragg markers correspond to Bi-I (at 1.2 GPa), Bi-III (at 6.0 GPa), and Bi-IV (at 12.9 GPa) phases. The derived unit cell volume (c) and lattice parameters (d) as a function of pressure. Solid line in (c) is a fit to the data using the third-order Birch-Murnaghan equation of state.

from hole to electron. In the case of $EuMnBi_2$ where the Fermi surface contains both electron and hole pockets [17], the sign of Hall resistivity depends on the relative magnitude of carrier concentrations and mobilities between the two. From the two-band model that we employed to analyze the MR and ρ_{xy} data of $EuMnBi_2$, it is revealed that although both hole and electron concentrations increase above 6 GPa, electron concentration becomes higher than hole. At the same time, the electron mobility also increases accompanied by the reduction of hole mobility. We propose that the valence change of the Eu ionic layer may introduce additional electron transfer to the Bi square nets. This charge transfer, in turn, modifies the Fermi surface, i.e., via the appearance of an electron pocket with large mobility on the Fermi surface that dominates the transport behavior above 6 GPa. Detailed density functional theory (DFT) calculations would clearly be beneficial to give insights on the possible Fermi surface reconstruction in $EuMnBi_2$ due to the Eu valence transition above 6 GPa.

IV. CONCLUSION

In summary, we report the high-pressure investigations on $EuMnBi_2$. We found that the Eu antiferromagnetic is enhanced under pressure up to 4 GPa, above which it

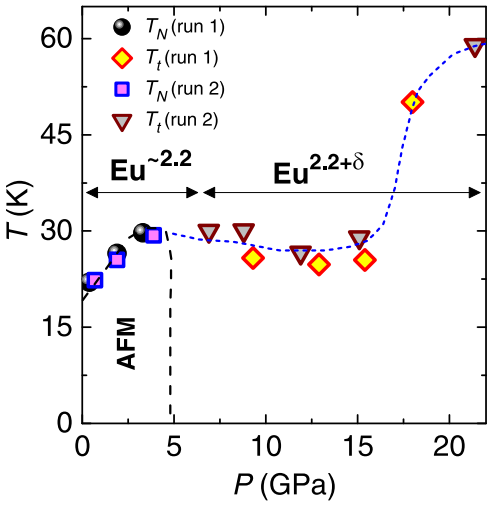

FIG. 7. Pressure-temperature phase diagram of $EuMnBi_2$ derived from the electrical resistivity. Dashed lines are guides to the eyes.

disappears. Another new low-temperature transition at $T_t \sim 28$ K appears on further compression above 6 GPa that we propose to be related to the Eu valence transition temperature toward a trivalent state. HERFD-XAS and XRD measurements at room temperature revealed a pressure-induced valence transition of Eu in $EuMnBi_2$ above 7 GPa without any structural transition. The sign change of Hall resistivity observed above 7 GPa suggests that the valence transition of Eu might induce a modification of the Fermi surface, in particular with the appearance of a new electron pocket with high mobility. Our work indicates that pressure can be used to effectively modify the interplay between magnetism, valence state, and band structure in the magnetic Dirac materials.

ACKNOWLEDGMENTS

We acknowledge support from the National Natural Science Foundation of China (NSFC) under Grants No. U1530402 and No. 11811530001. This work was supported by the U.S. DOE-BES, Division of Materials Science and Engineering, under Contract No. DE-SC0012704 (BNL materials synthesis). The synchrotron radiation experiments were performed at the BL10XU and BL39XU of SPring-8 with the approval of the Japan Synchrotron Radiation Research Institute (JASRI) under Proposals No. 2018A1374, No. 2018B1314, No. 2018B1310, and No. 2019A1412. We would like to thank Dr. Bo Gyu Jang for the useful discussions.

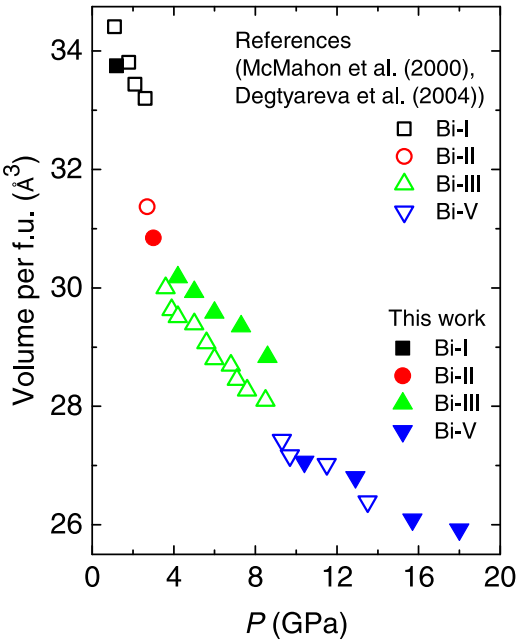

FIG. 8. The derived unit cell volume of the Bi impurity as a function of pressure. Solid symbols represent the unit cell volume of the Bi impurity in our $EuMnBi_2$ sample. Empty symbols represent the unit cell volume of pure Bi [38,39].

APPENDIX: PRESSURE DEPENDENCE OF THE UNIT CELL VOLUME OF THE Bi IMPURITY IN $EuMnBi_2$

In Fig. 8 we present the pressure dependence of the unit cell volume of the Bi impurity detected in our $EuMnBi_2$ sample. For comparison, the unit cell volume of pure Bi from previous reports [38,39] is also shown.

[1] O. Vafek and A. Vishwanath, Dirac fermions in solids: From high-T_c cuprates and graphene to topological insulators and Weyl semimetals, Annu. Rev. Condens. Matter Phys. **5**, 83 (2014).

[2] T. Wehling, A. Black-Schaffer, and A. Balatsky, Dirac materials, Adv. Phys. **63**, 1 (2014).

[3] J. Park, G. Lee, F. Wolff-Fabris, Y. Y. Koh, M. J. Eom, Y. K. Kim, M. A. Farhan, Y. J. Jo, C. Kim, J. H. Shim, and J. S. Kim, Anisotropic Dirac Fermions in a Bi Square Net of $SrMnBi_2$, Phys. Rev. Lett. **107**, 126402 (2011).

[4] J. K. Wang, L. L. Zhao, Q. Yin, G. Kotliar, M. S. Kim, M. C. Aronson, and E. Morosan, Layered transition-metal pnictide $SrMnBi_2$ with metallic blocking layer, Phys. Rev. B **84**, 064428 (2011).

[5] K. Wang, D. Graf, L. Wang, H. Lei, S. W. Tozer, and C. Petrovic, Two-dimensional Dirac fermions and quantum magnetoresistance in $CaMnBi_2$, Phys. Rev. B **85**, 041101(R) (2012).

[6] G. Lee, M. A. Farhan, J. S. Kim, and J. H. Shim, Anisotropic Dirac electronic structures of $AMnBi_2$ (A = Sr, Ca), Phys. Rev. B **87**, 245104 (2013).

[7] A. F. May, M. A. McGuire, and B. C. Sales, Effect of Eu magnetism on the electronic properties of the candidate Dirac material $EuMnBi_2$, Phys. Rev. B **90**, 075109 (2014).

[8] Y. F. Guo, A. J. Princep, X. Zhang, P. Manuel, D. Khalyavin, I. I. Mazin, Y. G. Shi, and A. T. Boothroyd, Coupling of magnetic order to planar Bi electrons in the anisotropic Dirac metals $AMnBi_2$ (A = Sr, Ca), Phys. Rev. B **90**, 075120 (2014).

[9] Y. J. Jo, J. Park, G. Lee, M. J. Eom, E. S. Choi, J. H. Shim, W. Kang, and J. S. Kim, Valley-Polarized Interlayer Conduction of Anisotropic Dirac Fermions in $SrMnBi_2$, Phys. Rev. Lett. **113**, 156602 (2014).

[10] Y. Feng, Z. Wang, C. Chen, Y. Shi, Z. Xie, H. Yi, A. Liang, S. He, J. He, Y. Peng, X. Liu, Y. Liu, L. Zhao, G. Liu, X. Dong, J. Zhang, C. Chen, Z. Xu, X. Dai, Z. Fang *et al.*, Strong anisotropy of Dirac cones in $SrMnBi_2$ and $CaMnBi_2$ revealed by angle-resolved photoemission spectroscopy, Sci. Rep. **4**, 5385 (2014).

[11] M. Chinotti, A. Pal, W. J. Ren, C. Petrovic, and L. Degiorgi, Electrodynamic response of the type-II Weyl semimetal $YbMnBi_2$, Phys. Rev. B **94**, 245101 (2016).

[12] H. Masuda, H. Sakai, M. Tokunaga, Y. Yamasaki, A. Miyake, J. Shiogai, S. Nakamura, S. Awaji, A. Tsukazaki, H. Nakao, Y. Murakami, T.-h. Arima, Y. Tokura, and S. Ishiwata, Quantum Hall effect in a bulk antiferromagnet $EuMnBi_2$ with magnetically confined two-dimensional Dirac fermions, Sci. Adv. **2**, e1501117 (2016).

[13] A. Wang, D. Graf, L. Wu, K. Wang, E. Bozin, Y. Zhu, and C. Petrovic, Interlayer electronic transport in $CaMnBi_2$ antiferromagnet, Phys. Rev. B **94**, 125118 (2016).

[14] A. Wang, I. Zaliznyak, W. Ren, L. Wu, D. Graf, V. O. Garlea, J. B. Warren, E. Bozin, Y. Zhu, and C. Petrovic, Magnetotransport study of Dirac fermions in $YbMnBi_2$ antiferromagnet, Phys. Rev. B **94**, 165161 (2016).

[15] A. Zhang, C. Liu, C. Yi, G. Zhao, T.-L. Xia, J. Ji, Y. Shi, R. Yu, X. Wang, C. Chen, and Q. Zhang, Interplay of Dirac electrons and magnetism in $CaMnBi_2$ and $SrMnBi_2$, Nat. Commun. **7**, 13833 (2016).

[16] J. Y. Liu, J. Hu, D. Graf, T. Zou, M. Zhu, Y. Shi, S. Che, S. M. A. Radmanesh, C. N. Lau, L. Spinu, H. B. Cao, X. Ke, and Z. Q. Mao, Unusual interlayer quantum transport behavior caused by the zeroth Landau level in $YbMnBi_2$, Nat. Commun. **8**, 646 (2017).

[17] S. Borisenko, D. Evtushinsky, Q. Gibson, A. Yaresko, K. Koepernik, T. Kim, M. Ali, J. van den Brink, M. Hoesch, A. Fedorov, E. Haubold, Y. Kushnirenko, I. Soldatov, R. Schäfer, and R. J. Cava, Time-reversal symmetry breaking type-II Weyl state in $YbMnBi_2$, Nat. Commun. **10**, 3424 (2019).

[18] X.-L. Qi and S.-C. Zhang, Topological insulators and superconductors, Rev. Mod. Phys. **83**, 1057 (2011).

[19] J. Alicea, New directions in the pursuit of Majorana fermions in solid state systems, Rep. Prog. Phys. **75**, 076501 (2012).

[20] C. Beenakker, Search for Majorana fermions in superconductors, Annu. Rev. Condens. Matter Phys. **4**, 113 (2013).

[21] M. Sato and Y. Ando, Topological superconductors: A review, Rep. Prog. Phys. **80**, 076501 (2017).

[22] H. Chen, L. Li, Q. Zhu, J. Yang, B. Chen, Q. Mao, J. Du, H. Wang, and M. Fang, Pressure-induced superconductivity in the antiferromagnetic Dirac material $BaMnBi_2$, Sci. Rep. **7**, 1634 (2017).

[23] K. Vinod, A. Bharathi, A. Satya, S. Sharma, T. Devidas, A. Mani, A. Sinha, S. Deb, V. Sridharan, and C. Sundar, Observation of superconductivity in $SrMnBi_2$ and Bi interface, Solid State Commun. **192**, 60 (2014).

[24] H. K. Mao, J. Xu, and P. M. Bell, Calibration of the ruby pressure gauge to 800 kbar under quasi-hydrostatic conditions, J. Geophys. Res. **91**, 4673 (1986).

[25] J. Rodriguez-Carvajal, Recent advances in magnetic structure determination by neutron powder diffraction, Phys. B: Condens. Matter **192**, 55 (1993).

[26] T. Roisnel and J. Rodriguez-Carvajal, WinPLOTR: A windows tool for powder diffraction pattern analysis, Mat. Sci. Forum **378-381**, 118 (2001).

[27] S. A. Medvedev, P. Naumov, O. Barkalov, C. Shekhar, T. Palasyuk, V. Ksenofontov, G. Wortmann, and C. Felser, Structure and electrical resistivity of mixed-valent $EuNi_2P_2$ at high pressure, J. Phys.: Condens. Matter **26**, 335701 (2014).

[28] F. Honda, K. Okauchi, Y. Sato, A. Nakamura, H. Akamine, Y. Ashitomi, M. Hedo, T. Nakama, T. Takeuchi, J. Valenta, J. Prchal, V. Sechovský, D. Aoki, and Y. Ōnuki, Pressure-induced valence change and moderate heavy fermion state in Eu compounds, Phys. B: Condens. Matter **536**, 182 (2018).

[29] H. Wada, M. F. Hundley, R. Movshovich, and J. D. Thompson, Pressure effect on the valence transition of $EuNi_2(Ge_{1-x}Si_x)$, Phys. Rev. B **59**, 1141 (1999).

[30] Y. Li, E. Wang, X. Zhu, and H.-H. Wen, Pressure-induced superconductivity in Bi single crystals, Phys. Rev. B **95**, 024510 (2017).

[31] H. J. Park, B. C. Park, M.-C. Lee, D. W. Jeong, J. Park, J. S. Kim, H. S. Ji, J. H. Shim, K. W. Kim, S. J. Moon, H.-D. Kim, D.-Y. Cho, and T. W. Noh, Electrodynamic properties of the semimetallic Dirac material $SrMnBi_2$: Two-carrier-model analysis, Phys. Rev. B **96**, 155139 (2017).

[32] Y.-Y. Wang, S. Xu, L.-L. Sun, and T.-L. Xia, Quantum oscillations and coherent interlayer transport in a new topological Dirac semimetal candidate $YbMnSb_2$, Phys. Rev. Mater. **2**, 021201(R) (2018).

[33] A. Wang, S. Baranets, Y. Liu, X. Tong, E. Stavitski, J. Zhang, Y. Chai, W.-G. Yin, S. Bobev, and C. Petrovic, Magnetic mixed valent semimetal $EuZnSb_2$ with Dirac states in the band structure, Phys. Rev. Research **2**, 033462 (2020).

[34] E. H. Putley, *The Hall Effect and Related Phenomena* (Butterworths, London, 1960).

[35] R. A. Smith, *Semiconductors* (Cambridge University Press, Cambridge, 1978).

[36] H. de Graaf, R. Thiel, and K. Buschow, On the valence of Eu in Eu-Pt compounds, Physica B+C **100**, 81 (1980).

[37] J. H. Chen, H. Iwasaki, and T. Ktkegawa, Crystal structure of the high pressure phases of bismuth Bi-III and Bi-III′ by high energy synchrotron x-ray diffraction, High Press. Res. **15**, 143 (1996).

[38] M. I. McMahon, O. Degtyareva, and R. J. Nelmes, Ba-IV-Type Incommensurate Crystal Structure in Group-V Metals, Phys. Rev. Lett. **85**, 4896 (2000).

[39] O. Degtyareva, M. I. MCMahon, and R. J. Nelmes, High-pressure structural studies of group-15 elements, High Press. Res. **24**, 319 (2004).

[40] F. Birch, Finite elastic strain of cubic crystals, Phys. Rev. **71**, 809 (1947).

[41] F. D. Murnaghan, Finite deformations of an elastic solid, Am. J. Math. **59**, 235 (1937).

[42] H. v. Löhneysen, A. Rosch, M. Vojta, and P. Wölfle, Fermi-liquid instabilities at magnetic quantum phase transitions, Rev. Mod. Phys. **79**, 1015 (2007).

[43] J. Guo, J. W. Simonson, L. Sun, Q. Wu, P. Gao, C. Zhang, D. Gu, G. Kotliar, M. Aronson, and Z. Zhao, Observation of antiferromagnetic order collapse in the pressurized insulator LaMnPO, Sci. Rep. **3**, 2555 (2013).

[44] P. G. Naumov, K. Filsinger, S. I. Shylin, O. I. Barkalov, V. Ksenofontov, Y. Qi, T. Palasyuk, W. Schnelle, S. A. Medvedev, M. Greenblatt, and C. Felser, Pressure-induced magnetic collapse and metallization of $TlFe_{1.6}Se_2$, Phys. Rev. B **96**, 064109 (2017).

[45] F. H. Yu, H. M. Mu, W. Z. Zhuo, Z. Y. Wang, Z. F. Wang, J. J. Ying, and X. H. Chen, Elevating the magnetic exchange coupling in the compressed antiferromagnetic axion insulator candidate $EuIn_2As_2$, Phys. Rev. B **102**, 180404(R) (2020).

[46] K. Matsubayashi, K. Munakata, M. Isobe, N. Katayama, K. Ohgushi, Y. Ueda, N. Kawamura, M. Mizumaki, N. Ishimatsu, M. Hedo, I. Umehara, and Y. Uwatoko, Pressure-induced changes in the magnetic and valence state of $EuFe_2As_2$, Phys. Rev. B **84**, 024502 (2011).

[47] H.-J. Hesse, R. Lübbers, M. Winzenick, H. Neuling, and G. Wortmann, Pressure and temperature dependence of the Eu valence in $EuNi_2Ge_2$ and related systems studied by Mössbauer effect, x-ray absorption, and x-ray diffraction, J. Alloys Compd. **246**, 220 (1997).

[48] F. Honda, K. Okauchi, A. Nakamura, D. Li, D. Aoki, H. Akamine, Y. Ashitomi, M. Hedo, T. Nakama, and Y. Ōnuki, Pressure-induced valence transition and characteristic electronic states in $EuRh_2Si_2$, J. Phys. Soc. Jpn. **85**, 063701 (2016).